Direct Measurement of Seismo-acoustic Wave Coupling

Eric Lysenko

A thesis report submitted to the faculty of

Brigham Young University

In partial fulfillment of the requirements for the degree of

Bachelor of Science

Tracianne Neilsen, Advisor

Department of Physics and Astronomy

Brigham Young University

June 2019

ABSTRACT

Title: Preliminary attempts to measure ground-radiated noise from exploding balloons

Authors: E. J. Lysenko, T. B. Neilsen

Department of Physics and Astronomy

Bachelor of Science

Seismo-acoustic coupling occurs when seismic wave propagation creates air-borne acoustic signals. Research is ongoing to determine methods to distinguish between sound due to seismo-acoustic coupling and purely air-borne transmission. In a field experiment, we detonated 17-inch balloons filled with a stoichiometric oxy-acetylene mix placed both on and in the ground. We attempted to isolate ground-radiated waves by constructing a portable soundproof box to deaden air-borne sound waves. The box was constructed from mass-loaded vinyl, soundproofing composite board, liquid nails, and green glue. This design incorporated soundproofing through decoupling, absorption, and insulation techniques. Signals observed from a microphone placed in the box are compared with those obtained on microphones outside the box at various heights. The initial blast wave was not evident inside the box. However, the loudest sound measured in the box matches a subsequent portion of signals on microphones near the ground. Testing in a reverberation chamber is done to measure the insertion loss of the box. The insertion loss is applied to our signals from the balloons. Our results did not indicate the presence of coupled waves. However, ongoing research may suggest this as a viable technique for isolating ground-borne acoustic waves.

Acknowledgments

Table of Contents

1. List of Figures

1 Introduction

1.1 Motivation

According to the Smithsonian institution, 60-80 volcanoes erupt every year[1]. Since the 2010 Iceland volcanic eruption, greater emphasis has been placed on aircraft safety with regard to volcanoes. Given that the ejecta from volcanoes has a lower melting point than the operating temperature of aircraft engines (Matoza *et al.* 2018a), volcanic eruptions pose a serious threat to operating aircraft. At present, we require visual confirmation of volcanoes to know how much ejecta and vapor is released into the atmosphere during an eruption. The delay this causes in rerouting air traffic can have catastrophic repercussions for aircraft in the vicinity of an eruption. Recent research has focused on using infrasound wave detection from volcanoes to ascertain the type of eruption taking place without visual confirmation (Matoza *et al.* 2018a). The overall goal of this research is to correspond infrasound waveforms to different volcanic eruptions so that visual confirmation is not necessary.

One method of researcher is to use scale model eruptions to approximate volcanic blasts. This provides a more controlled way to investigate volcanic eruptions through buried explosives. By using buried explosives, researchers can make approximations of acoustic and seismic signals generated by different volcanoes based on their eruptions. Examples of scale-model experiments have been used by Bowman *et al.* (2014), Ohba *et al.* (2002), Spina *et al.* (2018), and Taddeucci *et al.* (2013).

---

[1] Smithsonian Institution National Museum of Natural History Global Volcanism program. Retrieved May 2, 2019, from https://volcano.si.edu/faq/index.cfm?question=historicalactivity

In Summer 2018, we teamed with Robin Matoza's group at UCSB to participate in two scale-model explosion experiments: one with oxy-acetylene-filled balloons and another with buried C-4-like explosives. The purpose of these experiments was to record the acoustic signal of different explosion sequences and the effect of crater size. The data and analysis of these scale-model experiments will hopefully aid in characterizing volcanic eruptions from the infrasound they emit.

My research in these fields is measuring the seismo-acoustic coupling that occurs as a result of the blasts. I did this with a portable soundproof apparatus that blocks airborne acoustic waves in order to observe acoustic waves generated by seismic waves.

1.2 Infrasound Background

One way to monitor volcanoes from a safe distance is by studying infrasound. An infrasound wave is an airborne acoustic wave with a frequency < 20Hz. Infrasound can travel thousands of kilometers due to low atmospheric absorption and atmospheric refraction effects. The long-range nature of infrasound also makes it useful for detecting nuclear explosions, which is why the International Monitoring System (IMS) is maintained (See Fig. 1). Though the IMS is explicitly in place for detecting nuclear explosions, it could be used to detect and provide early warning for volcanic blasts that pose serious threat to aircraft by monitoring their infrasound (Matoza *et al.* 2017).

Previous research shows the usefulness of infrasound in characterizing volcanic eruptions. Many studies have characterized the sound from Strombolian (Vergniolle and Brandeis 1994 and 1996, Jolly *et al.* 2017), Plinian (Fee *et al.* 2010a), and Vulcanian explosions (Matoza *et al.* 2018b, Anderson *et al.* 2019, Marchetti 2009), as well as degassing explosions

(Johnson and Lees 2000), volcanic tremors (Fee *et al.* 2010b, Fee *et al.* 2017a), and rock fall (Moran *et al.* 2008). Connections have also been made between infrasound and eruption mass (Fee *et al.* 2017b), velocity (Matoza *et al.* 2013b) and plume height (Caplan-Auerbach *et al.* 2010). The infrasound from volcanic jetting (Mckee *et al.* 2017)—where pressurized air is released—has been shown to have the same statistical distribution as the noise from solid rocket motors and afterburning military aircraft.
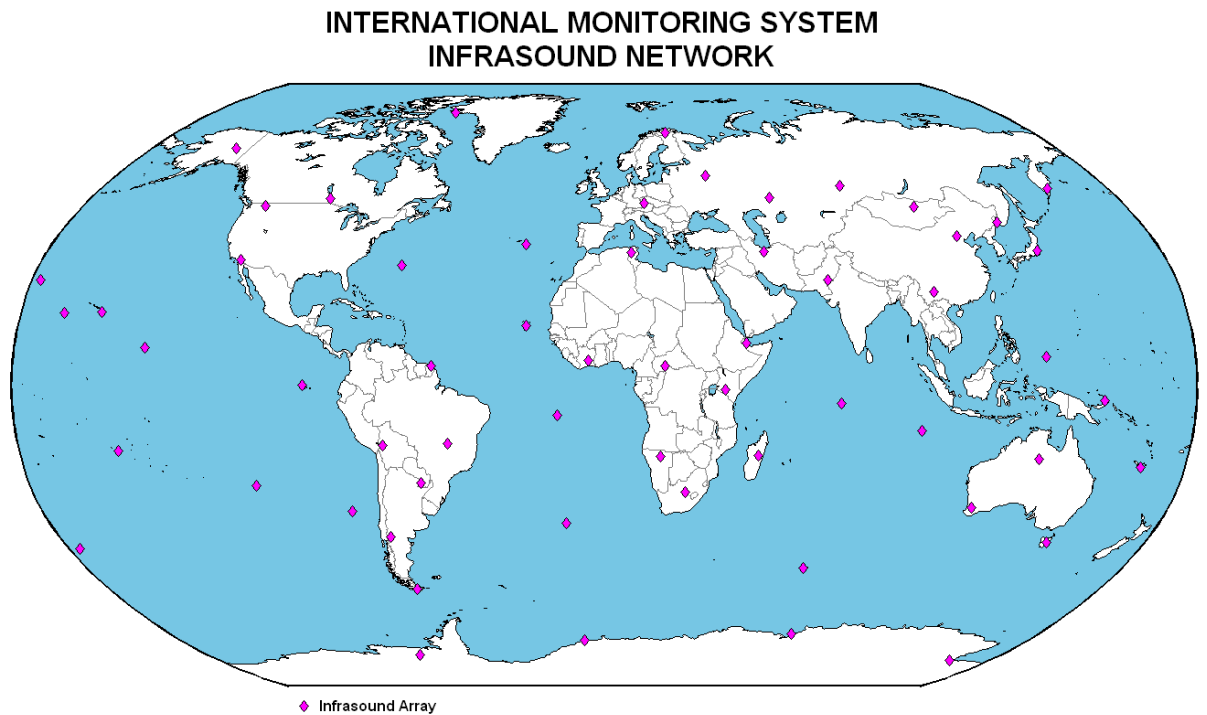
INTERNATIONAL MONITORING SYSTEM
INFRASOUND NETWORK

Figure 1 Map of Global Infrasound Detection Network

1.3 Acoustic Coupling

This paper focuses on one aspect of volcanic research effort: seismo-acoustic coupling. The two types of seismo-acoustic coupling occur: when airborne acoustic waves strike the ground and create seismic waves (air-to-ground coupling) and the transference of acoustic energy from seismic waves to create airborne acoustic waves (ground-to-air coupling). Evidence of both types of seismo-acoustic coupling can be found by examining the cross-correlation (Ichihara *et al.* 2012) and coherence (Matoza *et al.* 2018c) of the vertical seismic velocity and infrasound signals, as well as the alignment of the vertical seismic displacement with the infrasound (Matoza *et al.* 2019).

The air-to-ground coupling, generated by elevated sources, has been studied on both regional and local scales (Matoza *et al.* 2018d) to monitor eruption tremors (Matoza and Fee 2014), and is now used for eruption detection at the Alaska Volcano Observatory (Fee *et al.* 2016). The frequency dependence of air-to-ground coupling has also been studied (Bass *et al.* 1980). Ground-to-air coupling from compressional and shear seismic waves and leaky Rayleigh waves have been identified,(Matoza *et al.* 2009) and are important to link infrasonic wave patterns with specific types of volcanic eruptions (Matoza *et al.* 2015). Ground-to-air coupling from these sources has also been used for signal detection and localization (Mckee *et al.* 2018). An example of ground-to-air coupling is shown in Fig. 2. It shows the outward propagation of a seismic wave and the coupling that it generates.

In the remainder of this paper we focus on ground-to-air seismo-acoustic coupling and how to quantify it. Measuring the coupling is necessary for volcanic research and is thus an area of interest in our scale model research. Our experiment aims to help us understand if coupling is

a negligible source of acoustic energy or how the coupled sound contributes to the overall

waveforms from explosions. We do this by attempting to filter out all other airborne noise with a

soundproof apparatus and taking direct measurements of the coupled waves.
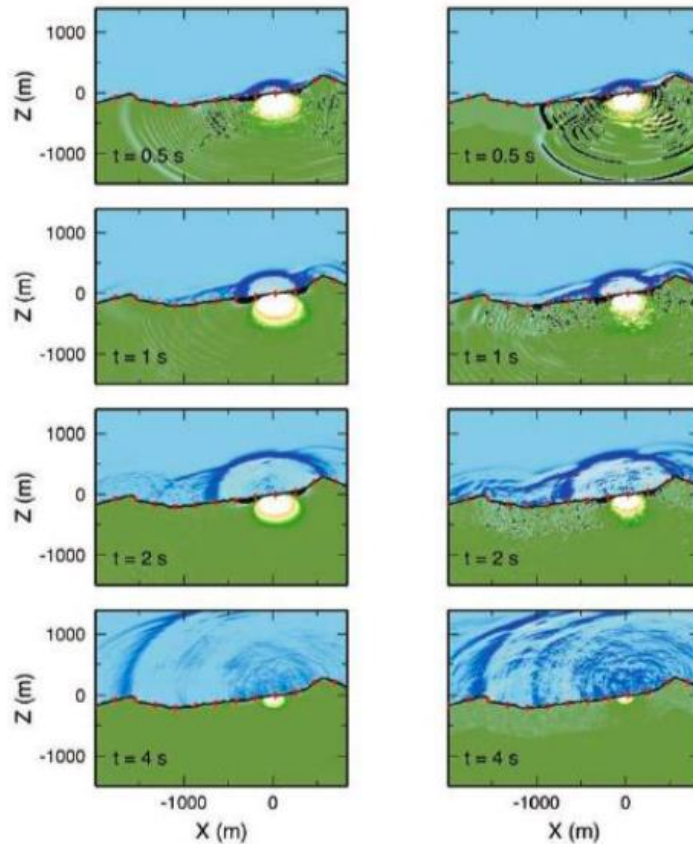
Figure 2 Shows the ground-to-air coupling effect as seismic waves propagate away from volcanic blast. Adapted from Matoza *et al.* (2009) Fig 10. Used with permission

1.4 Previous Research at BYU

Work done by Drs. Gee and Neilsen at BYU have already contributed to the field of

volcanic infrasound. In one paper (Fee *et al.* 2013), they showed that the statistics of the

infrasound during the jetting phase of a volcano are the same as those at higher frequencies for

solid rocket motors and high-performance military aircraft. The other paper (Matoza *et al.* 2013a) showed that the common monopole assumption used to estimate the power of a volcano is incorrect if the sound radiated has a directionality.

Brigham Young has also done work with the oxy-acetylene balloons (Macedone *et al.* 2014) to explore nonlinear propagation (Young *et al.* 2014) and Mach stems (Leete *et al.* 2015). However, this research is the first time oxy-acetylene balloons have been ignited on or in the ground and the first research at BYU on the seismo-acoustic coupling due to oxy-acetylene balloons.

1.5 Overview

The goal of my research is to find evidence of ground-to-air seismo-acoustic coupling when balloons filled with oxy-acetylene are detonated in the ground. We attempt to do this using a soundproof box to filter out the airborne acoustic signal generated by the explosions in order to take direct measurement of coupled waves. Section 2 describes the methods used to create the box and the experimental setups. Section 3 explains our results and conclusions.

2 Methods

Methods for measuring the seismo-acoustic coupling are reported in this chapter. First, information regarding the plan, design, and construction of our soundproof box apparatus is presented. The experimental setup for the field test and reverberations chamber test are then described.

2.1 Box Design

The box was designed to insulate a microphone from airborne waves and isolate only ground-to-air coupled waves, as shown in the Fig. 3. Airborne waves encountering the surface of the apparatus are reflected and deadened so that the microphone housed within only detects coupled waves.
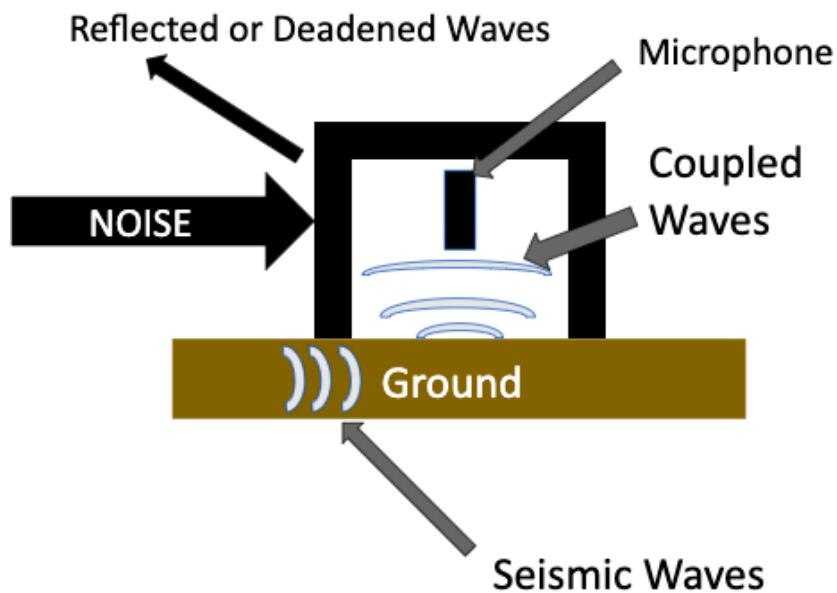
Figure 3 – Apparatus setup showing attenuation of airborne acoustic waves and ground-air acoustic coupling within the box.

2.1.1 Construction

The box was designed to limit the amount of air-borne noise entering the box. The box was composed of 20-lb of mass loaded vinyl (MLV) at 1-lb/ft^2, 4-ft^2 of Home Depot soundproofing board, liquid nails and wood glue to glue the sheets together, and duct tape to keep the MLV from sliding out of the box. Exact instructions for making the box are provided in Appendix A. The design incorporated three important aspects of soundproofing: high mass, mechanical decoupling, and absorption. The high mass component comes from using MLV. The mechanical decoupling effect was created by placing the MLV sheets tightly without adhesive. Absorption was included by incorporating the soundproof boards, which are good insulators. The following figures show side and bottom views of the box. The box was approximately 1'x1'x 8''. The MLV penetrates past the base of the soundproofing board by 2''. There is approximately 2'' of MLV between ¾'' soundproofing boards that constitute each wall. Fig. 4 shows bottom and side views of the box.

Figure 4- Bottom and side views of the box. Duct tape was used to keep sheets from sliding out.

2.2 Experiments

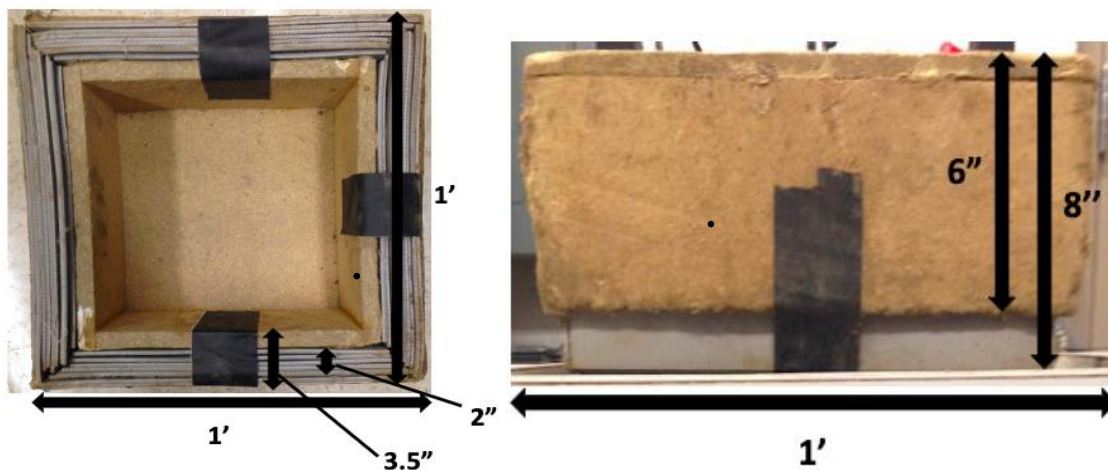This section describes the setup and data acquired from the pretest (Exploding Balloon Test), and measurements taken in the BYU reverberation chamber to quantify the random-incidence insertion loss of the box.

2.2.1 Exploding Balloon Test

2.2.1.1 Purpose

The exploding balloon test was a pretest for the Geohazards workshop in Buffalo in July 2018. This pretest was important because we needed to be comfortable with the equipment and able to set it up in a timely manner at the actual test in Buffalo. We practiced setting up our microphone configuration and recorded sound pressure level (SPL) data for each balloon explosion.

Weather conditions and location were ideal for our balloon test. The test took place in a flat, grassy field in South Provo on July 11, 2018. The weather during the pretest was measured using Kestral 5500 weather meters. The temperature was ~29 C, wind speed between 1 and 2.65 knots, humidity ~ 36%, and pressure was ~ 865 millibar. A detailed hour-by-hour summary of these conditions can be found in Appendix B.

The experimental setup included a microphone arc array around the craters (craters are areas the balloons were detonated) and a linear microphone array from the craters as shown in Fig. 5. The soundproof box was placed 100 m away from the blast along the linear array, and an additional microphone was placed 3 feet south of the box (see Fig. 5). Both microphones were supported 2-3 mm from the ground with inverted tripods constructed at BYU.

The microphone placed next to the box was to compare the signals inside and out of the box. In a later test, we calculated the insertion loss of the box and applied it to the signal of the microphone outside of the box. This would tell us if the box was acting like a low-pass filter or picking up another source of acoustic energy.
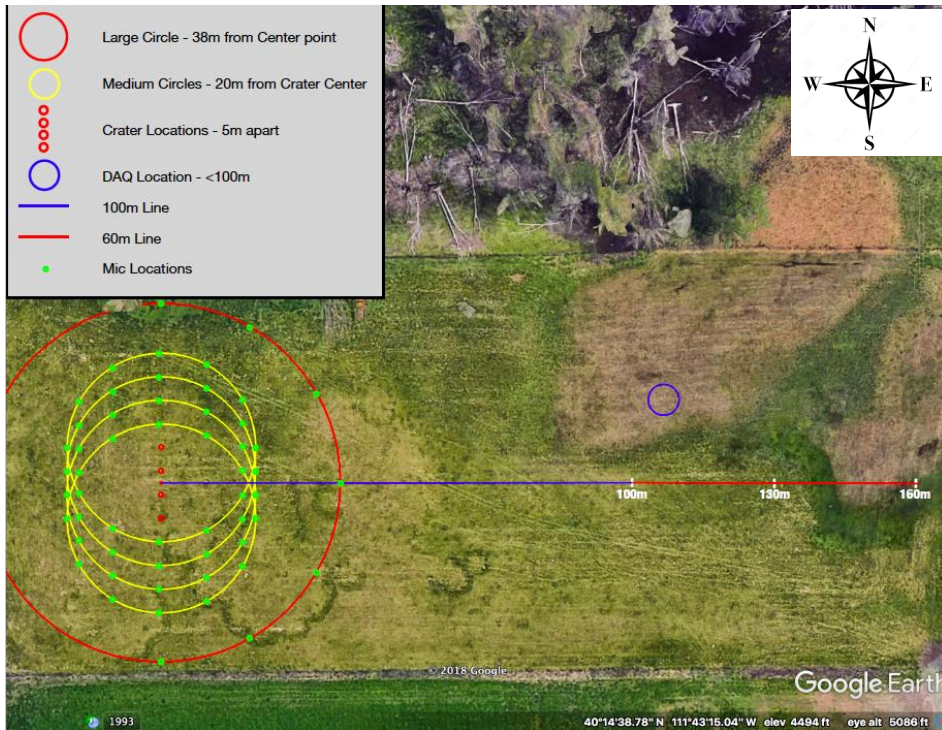
Figure 5- Google Map view of the Exploding Balloons Test. The yellow circles indicate the circular array around each blast. The Red circle indicates the arc array around all four blasts. The red line shows the linear array. The box was placed at 100 m.

2.2.1.2   The Balloons

During the pretest, balloons were filled with a stoichiometric oxy-acetylene mix to create large explosions. Exploding oxy-acetylene balloons are good models for large explosions (Young *et al.* 2015, Leete *et al.* 2015), making them ideal for our test. Balloons were set up in different craters of varying depth and size so we could see the impact of crater shape on acoustic

signals. The balloons were detonated via radio transmitter connected to a model rocket ignition match. One of the balloons is shown in Fig. 6. The plastic wrap in this figure was used to keep them from popping on the grass or from being blown away.

Figure 6 – Balloon shown on ground covered in plastic wrap to keep it from popping on the grass and also to keep the wind from blowing it away

2.2.1.3   The Balloon Craters
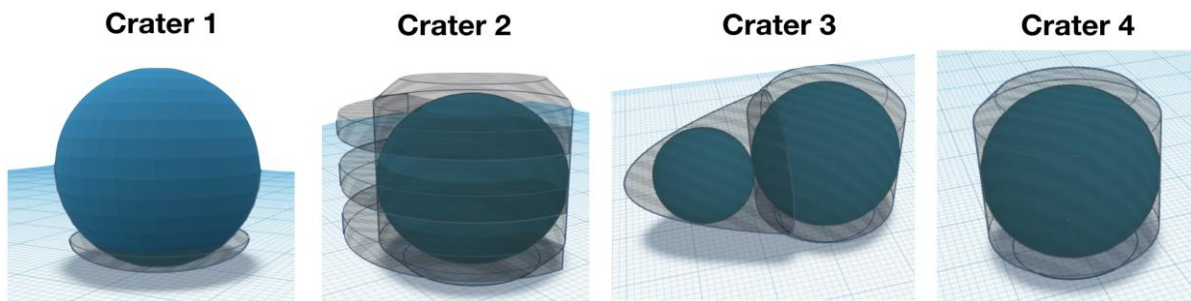
Figure 7- 3D rendering of balloons in three 'crater' positions. Crater 1 is in a slight ground depression, Crater 2 is completely buried with three notches in the side of the crater for directionality, Crater 3 has two buried balloons, and Crater 4 is in an unmodified crater.

To study the impact of the crater shape on the acoustical signals, balloons were placed in four configurations or "craters," as shown in Fig. 7. Crater 1 corresponded to a balloon placed on the ground and served as a control so we would know how explosions sound without obstruction

from being buried in the ground. Crater 2 had three notches to test the directionalization of the

fractured soil (Isakov *et al.* 1983). Crater 3's setup was used to create a coupled explosion from

both balloons. Crater 4 was another control to see the effect of crater shape on the acoustic

signals.

2.2.1.4   The Microphones

The box microphone and the adjacent ground microphone were ½ inch GRAS pre-

polarized free-field microphones. The microphones had a range from 20Hz to 20kHz, a dynamic

range of 15 dB(A) to 148 dB, and ~56 mV/Pa sensitivity. Each was set up in an inverted tripod

as shown in Fig. 8-a. The box in the microphone was also set on a tripod inside of a 6" deep

square hole that the box could fit in, as shown in Fig. 8-b. The hole was then covered by the box

and the sides were packed (Fig. 8-c).

Figure 8- From left to right: (a) a ground microphone in an inverted tripod that was placed next to the box. (b) a ground mic in an inverted microphone in the uncovered box hole. (c) the box placed in the ground

2.2.1.5   Results

The acoustic signals were recorded via microphone connected to a DAQ (National Instruments PXI-1042 at 204.8kHz sampling rate) that recorded the data in Labview. The data was then analyzed in MATLAB. Fig. 9 shows the pressure waveform received on the ground microphones outside (red) and inside (black) the box. Obviously, the box dampened a significant amount of the air-born sound. The question remained as to if the microphone in the box was simply detecting air-borne sound filtered by the box or sound radiated from a passing seismic wave. The next phase of our testing would see if the box mic behaved like a low-pass filter, or if the sound levels were due to coupling.
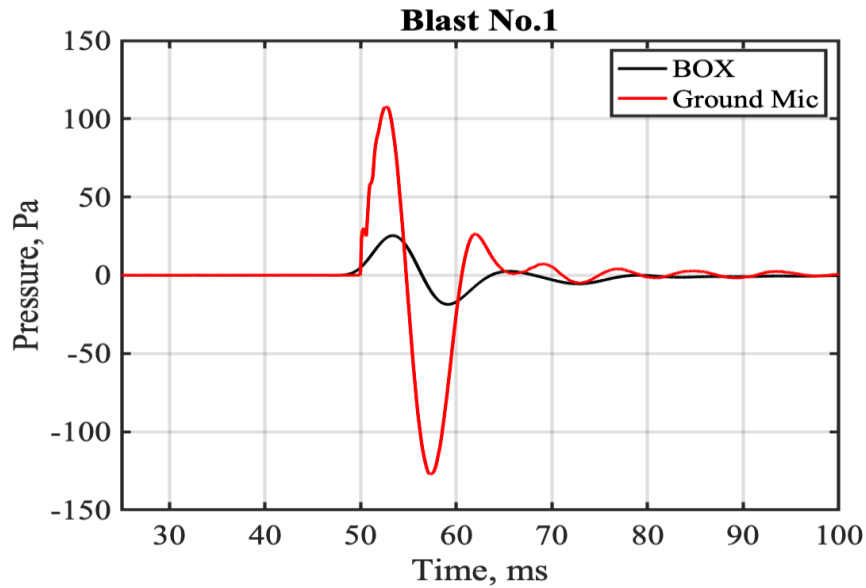

Figure 9- Waveform of a pretest blast with ground mic and box mic (in code set iich = [16:17]+1;). Distance 100m. Code for this figure can be found in Appendix C.

2.2.2 Reverberation Chamber Test

2.2.2.1 Purpose

The random insertion loss of our box was measured via a test in the reverberation chamber. By determining the sound level reduction due to the box, we could see if our box signal picked up coupled waves in the balloons test or not. If more sound was in the box than expected after the insertion loss was accounted for, then we could successfully conclude that the sound picked up was from coupled waves.

2.2.2.2 Setup

Our reverberation chamber test needed to resemble our exploding balloons test for its insertion loss to be useful in the balloons test. To replicate the box being fully insulated, the box was placed on a memory foam pad. However, the foam was not completely compressed without additional weight on top. A concrete block was added on top of the box to fully compress the foam, as shown in Fig. 10. The test was carried out with and without a concrete weight on top of the box to approximate upper and lower bounds of noise filtering. One mic was placed in the box while the other three were placed off to the side. Microphones were suspended over the ground using inverted tripods constructed in our machine shop at BYU. The microphones were suspended between 1 and 3 mm above the ground. Insertion loss was measured from a starter pistol because it resembled the blasts from our pretest.
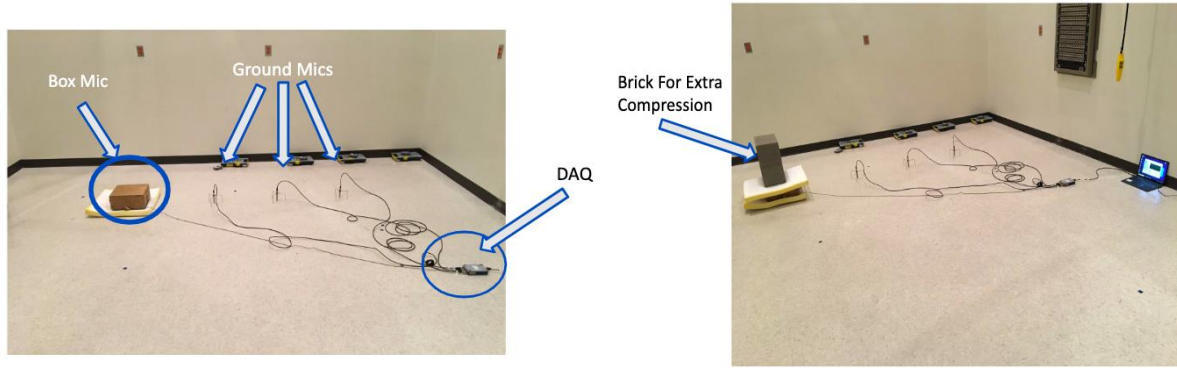
Figure 10- The setup in the reverberation chamber. On the left shows the setup with no concrete on top of the box. The right shows the setup with the concrete on the box.

2.2.2.3 Data

We recorded measurements with a DAQ (National Instruments PXI-1042 at 51.2kHz sampling rate) and Labview Software developed in the BYU physics department by Dr. Gee. We converted the frequency spectra of the starter pistol shots to a one-third octave (OTO) band spectra spectrum with MATLAB and generated two plots (Fig. 11): one modeling the spectrum with concrete on the box and the other without. The graph with 'YES Concrete On Box' shows that the box begins filtering noise at 10Hz and becomes more effective at soundproofing as frequency increases. The improvement in sound filtering increases at a somewhat constant rate as frequency increases. The graph with 'NO Concrete on Box' shows the box beginning to filter noise at ~50Hz and provides less reduction in overall sound level. These data were then used to calculate the insertion loss of the system.
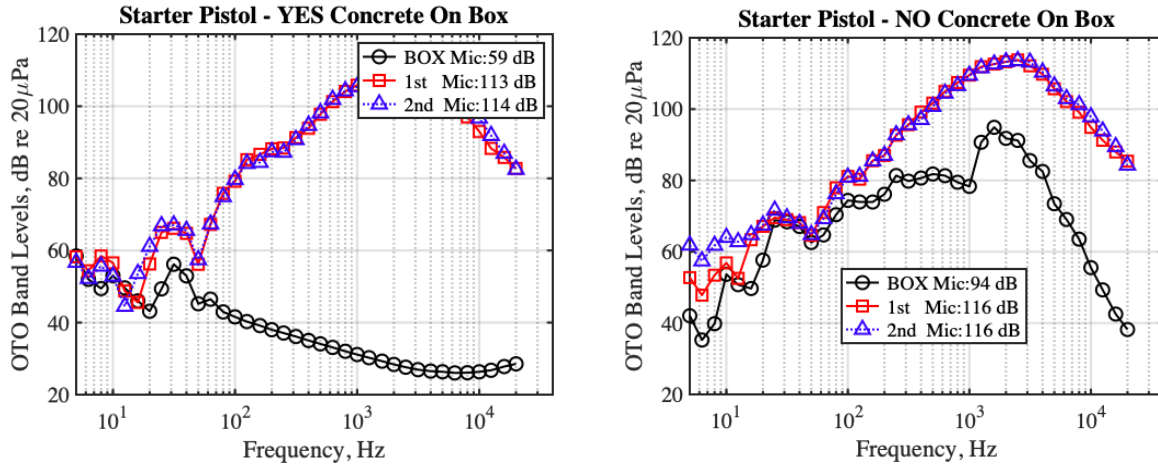
Figure 11- The one-third-octave (OTO) band levels from a gunshot in the reverberation chamber. The black lines show the OTO band levels of the microphone in the box. Code for these figures can be found in Appendix C.

2.3 Insertion Loss

2.3.1 Purpose

Insertion Loss is the reduction in noise level due to the addition of a barrier or enclosure. Measuring this value tells us if the signal in our box during the pretest was due to coupling or acoustic signals penetrating the box.

2.3.2 Method

In our experiment we estimated random incidence insertion loss because the sound field was diffuse in the reverberation chamber. The insertion loss from our reverberation chamber test indicates how well the box attenuates airborne impulse signals. Insertion loss is measured by

$$IL(dB) = 10 * \log_{10}(P_T/P_R),$$

where P_T is the load before and enclosure and P_R is load after the enclosure. The signal from the box is given as P_R and the average signal from the three outer microphones is given as P_T. By completing the experiment with and without weight on the box we approximated upper and lower bounds of insertion loss. This calculation was done using MATLAB, and the resulting insertion loss is shown in Fig. 12.
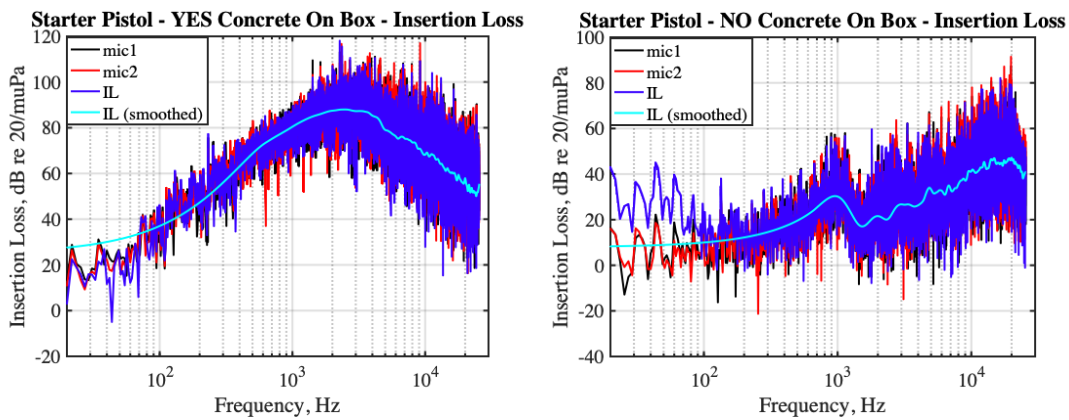
Figure 12- Graphs of the insertion loss (IL) from the two setups in the reverberation chamber. On the left, the IL with concrete weight on the box. On the right, the IL without concrete. The IL with the concrete was considerably greater than without. Code for these figures can be found in Appendix C.

3 Results and Conclusions

The results of applying the insertion loss to pretest are presented and analyzed. The box acts as a low-pass filter for the pretest, and no seismo-acoustic coupling is detected.

3.1 Results

The calculated insertion loss was applied to the ground mic signal with MATLAB. Fig. 13 shows the SPL (Sound Pressure Level) and OTO (one-third-octave) band levels of the ground mic signal with the insertion loss applied. The signal falls within the proposed upper and lower limits of insertion loss.
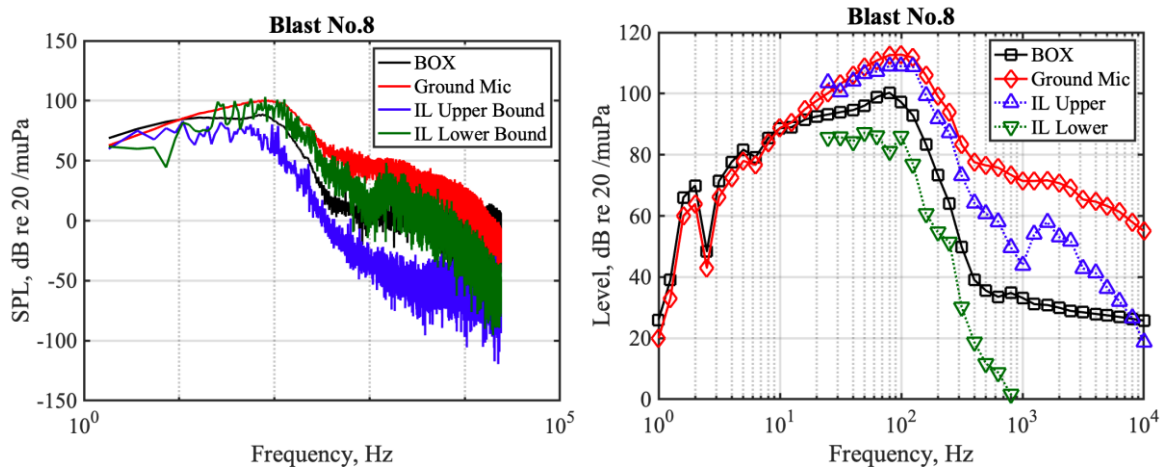
Figure 13 – The SPL (left) and OTO band levels (right) with the insertion loss applied to the ground microphone adjacent to the box. The signal falls within the proposed upper and lower limits of insertion loss, hence we cannot assume that we detected coupling.

3.2 Analysis

The box signal in Fig. 13 (shown as black squares) lies well between the insertion loss tolerances from 20Hz and above, which are shown with the blue triangles and green inverted triangles. The insertion loss signals begin at 20Hz because the subwoofer used in the reverberation chamber test was only reliable down to 20Hz. Notwithstanding, the calculated insertion loss at 20Hz is close to zero, which implies that the box is less effective at filtering out infrasound. The box appears to be receiving another source of sound when frequency > 8K. However, the excess high-frequency energy in the box could be due to scattering.

3.3 Conclusion

The goal of this work was to construct and use a sound-proof box to identify ground-to-air seismo-acoustic coupling from impulsive sources. The box was constructed as a portable means of measuring coupling in the field. In our test, a microphone was placed on the ground and covered by the box. Another microphone stood adjacent and was used to compare SPL within and without the box. Oxy-acetylene balloons were detonated in various configurations and the SPL data collected. Random incidence insertion loss was also measured in a separate test and applied to our data to see if the box acted like a low-pass filter or detected coupled waves.

The signal received on the microphone inside the box during the pretest falls within the upper and lower bounds of the box's insertion loss. Thus, in the pretest, the box appears to behave like a low-pass filter.

Although we did not find evidence of coupling in this experiment, I learned a lot by designing, constructing, and testing my soundproof box. I found that portable noise proof devices

are hard to create because deadening low frequency noises and audible frequency noises requires lots of space within the apparatus. This is a major design hurdle for any portable soundproofing device.

3.4 Future Work

By estimating the insertion loss of the box, we showed that the box acts as a low-pass filter. Though there was no evidence of coupling in this experiment, preliminary data from a recent field test (Geohazards workshop in Buffalo, NY) do provide evidence of coupling. This may have been due to differences in soil composition, the depth of the explosives, relative distance from the blasts, and the depth the box was buried. Future work will focus on analyzing the data from the Geohazards workshop for more evidence of coupling by the same method of insertion loss used here.

4 References

Anderson, J. F., Johnson, J. B., Steele, A. L., Ruiz, M. C., & Brand, B. D. (2018). Diverse eruptive activity revealed by acoustic and electromagnetic observations of the 14 July 2013 intense vulcanian eruption of Tungurahua volcano, Ecuador. Geophysical Research Letters, 45, 2976– 2985.

Bass, H. E., Bolen, L. N., Cress, D., Lundien, J., & Flohr, M. (1980). Coupling of airborne sound into the earth: Frequency dependence. *The Journal of the Acoustical Society of America*, *67*(5), 1502-1506.

Bowman, D. C., Taddeucci, J., Kim, K., Anderson, J. F., Lees, J. M., Graettinger, A. H., ... & Valentine, G. A. (2014). The acoustic signatures of ground acceleration, gas expansion, and spall fallback in experimental volcanic explosions. *Geophysical Research Letters*, *41*(6), 1916-1922.

Caplan-Auerbach, J., Bellesiles, A., & Fernandes, J. K. (2010). Estimates of eruption velocity and plume height from infrasonic recordings of the 2006 eruption of Augustine Volcano, Alaska. *Journal of Volcanology and Geothermal Research*, *189*(1-2), 12-18.

Fee, D., Garces, M., & Steffke, A. (2010a). Infrasound from Tungurahua volcano 2006–2008: Strombolian to Plinian eruptive activity. *Journal of Volcanology and Geothermal Research*, *193*(1-2), 67-81.

Fee, D., Steffke, A., & Garces, M. (2010b). Characterization of the 2008 Kasatochi and Okmok eruptions using remote infrasound arrays. Journal of Geophysical Research: Atmospheres, 115(D2).

Fee, D., Matoza, R. S., Gee, K. L., Neilsen, T. B., and Ogden, D. E. (2013), Infrasonic crackle and supersonic jet noise from the eruption of Nabro Volcano, Eritrea, *Geophys. Res. Lett.*, 40, 4199– 4203, doi:10.1002/grl.50827.

Fee, D., Haney, M., Matoza, R., Szuberla, C., Lyons, J., & Waythomas, C. (2016). Seismic envelope-based detection and location of ground-coupled airwaves from volcanoes in Alaska. *Bulletin of the Seismological Society of America*, *106*(3), 1024-1035.

Fee, D., Haney, M. M., Matoza, R. S., Van Eaton, A. R., Cervelli, P., Schneider, D. J., & Iezzi, A. M. (2017a). Volcanic tremor and plume height hysteresis from Pavlof Volcano, Alaska. Science, 355(6320), 45-48.

Fee, D., Izbekov, P., Kim, K., Yokoo, A., Lopez, T., Prata, F., ... & Iguchi, M. (2017b). Eruption mass estimation using infrasound waveform inversion and ash and gas measurements: Evaluation at Sakurajima Volcano, Japan. *Earth and Planetary Science Letters*, *480*, 42-52.

Ichihara, M., Takeo, M., Yokoo, A., Oikawa, J., and Ohminato, T. (2012), Monitoring volcanic activity using correlation patterns between infrasound and ground motion, Geophys. Res. Lett., 39, L04304, doi:10.1029/2011GL050542.

Isakov, A. L. (1983). Directed fracture of rocks by blasting. *Journal of Mining Science*, *19*(6), 479-488.

Johnson, J. B., & Lees, J. M. (2000). Plugs and chugs—seismic and acoustic observations of degassing explosions at Karymsky, Russia and Sangay, Ecuador. Journal of Volcanology and Geothermal Research, 101(1-2), 67-82.

Jolly, A. D., Matoza, R. S., Fee, D., Kennedy, B. M., Iezzi, A. M., Fitzgerald, R. H., ... & Johnson, R. (2017). Capturing the acoustic radiation pattern of strombolian eruptions using infrasound sensors aboard a tethered aerostat, Yasur volcano, Vanuatu. *Geophysical Research Letters*, *44*(19), 9672-9680.

Leete, K. M., Gee, K. L., Neilsen, T. B., & Truscott, T. T. (2015). Mach stem formation in outdoor measurements of acoustic shocks. *The Journal of the Acoustical Society of America*, *138*(6), EL522-EL527.

Macedone, J. H., Gee, K. L., & Vernon, A. J. A. (2014). Managing Auditory Risk from Acoustically Impulsive Chemical Demonstrations. *Journal of Chemical Education*, *91*(10), 1661-1666.

Marchetti, E., Ripepe, M., Harris, A. J. L., & Delle Donne, D. (2009). Tracing the differences between Vulcanian and Strombolian explosions using infrasonic and thermal radiation energy. *Earth and Planetary Science Letters*, *279*(3-4), 273-281.

Matoza, R. S., Garcés, M. A., Chouet, B. A., D'Auria, L., Hedlin, M. A., Groot-Hedlin, D., & Waite, G. P. (2009). The source of infrasound associated with long-period events at Mount St. Helens. *Journal of Geophysical Research: Solid Earth*, *114*(B4).

Matoza, R. S., Shearer, P. M., Lin, G., Wolfe, C. J., & Okubo, P. G. (2013a). Systematic relocation of seismicity on Hawaii Island from 1992 to 2009 using waveform cross correlation and cluster analysis. *Journal of Geophysical Research: Solid Earth*, *118*(5), 2275-2288.

Matoza, R. S., Fee, D., Neilsen, T. B., Gee, K. L., & Ogden, D. E. (2013b). Aeroacoustics of volcanic jets: Acoustic power estimation and jet velocity dependence. *Journal of Geophysical Research: Solid Earth*, *118*(12), 6269-6284.

Matoza, R. S., and Fee, D. (2014), Infrasonic component of volcano-seismic eruption tremor, Geophys. Res. Lett., 41, 1964– 1970, doi:10.1002/2014GL059301.

Matoza, R. S., Green, D. N., Le Pichon, A., Fee, D., Shearer, P., Mialle, P., & Ceranna, L. (2016). Automated detection and cataloging of global explosive volcanism using the International Monitoring System infrasound network. *The Journal of the Acoustical Society of America*, *139*(4), 2098-2098.

Matoza, R. S., Green, D. N., Pichon, A. Le, Shearer, P. M., Fee, D., Mialle, P., and Ceranna, L. (2017), Automated detection and cataloging of global explosive volcanism using the International Monitoring System infrasound network, J. Geophys. Res. Solid Earth, 122, 2946– 2971, doi:10.1002/2016JB013356.

Matoza, R. S., & Fee, D. (2018a). The inaudible rumble of volcanic eruptions.

Matoza, R. S., Fee, D., Green, D. N., Le Pichon, A., Vergoz, J., Haney, M. M., ... & McKee, K. (2018b). Local, regional, and remote seismo-acoustic observations of the April 2015 VEI 4 eruption of Calbuco volcano, Chile. *Journal of Geophysical Research: Solid Earth*, *123*(5), 3814-3827.

Matoza, R. S., Fee, D., Green, D. N., Le Pichon, A., Vergoz, J., Haney, M. M., *et al.* (2018c). Local, regional, and remote seismo-acoustic observations of the April 2015 VEI 4 eruption of Calbuco volcano, Chile. Journal of Geophysical Research: Solid Earth, 123, 3814– 3827. https://doi.org/10.1002/2017JB015182

Matoza, R. S., Fee, D., Green, D. N., Le Pichon, A., Vergoz, J., Haney, M. M., *et al.* (2018d). Local, regional, and remote seismo-acoustic observations of the April 2015 VEI 4 eruption of Calbuco volcano, Chile. Journal of Geophysical Research: Solid Earth, 123, 3814– 3827. https://doi.org/10.1002/2017JB015182

Matoza, R. S., Arciniega-Ceballos, A., Sanderson, R. W., Mendo-Pérez, G., Rosado-Fuentes, A., & Chouet, B. A. (2019). High-broadband seismoacoustic signature of Vulcanian explosions at Popocatépetl volcano, Mexico. Geophysical Research Letters, 46, 148– 157. https://doi.org/10.1029/2018GL080802

McKee, K., Fee, D., Yokoo, A., Matoza, R. S., & Kim, K. (2017). Analysis of gas jetting and fumarole acoustics at Aso Volcano, Japan. *Journal of Volcanology and Geothermal Research*, *340*, 16-29.

McKee, K., Fee, D., Haney, M., Matoza, R. S., & Lyons, J. (2018). Infrasound Signal Detection and Back Azimuth Estimation Using Ground‐Coupled Airwaves on a Seismo‐Acoustic Sensor Pair. *Journal of Geophysical Research: Solid Earth*, *123*(8), 6826-6844.

Moran, S. C., Matoza, R. S., Garcés, M. A., Hedlin, M. A. H., Bowers, D., Scott, W. E., Sherrod, D. R., and Vallance, J. W. (2008), Seismic and acoustic recordings of an unusually large rockfall at Mount St. Helens, Washington, Geophys. Res. Lett., 35, L19302, doi:10.1029/2008GL035176.

Ohba, T., Taniguchi, H., Oshima, H., Yoshida, M., & Goto, A. (2002). Effect of explosion energy and depth on the nature of explosion cloud: A field experimental study. *Journal of Volcanology and Geothermal Research*, *115*(1-2), 33-42.

Spina, L., Morgavi, D., Cannata, A., Campeggi, C., & Perugini, D. (2018). An experimental device for characterizing degassing processes and related elastic fingerprints: Analog volcano seismo-acoustic observations. *Review of Scientific Instruments*, *89*(5), 055102.

Taddeucci, J., Sesterhenn, J., Scarlato, P., Stampka, K., Del Bello, E., Pena Fernandez, J. J., & Gaudin, D. (2014). High-speed imaging, acoustic features, and aeroacoustic computations of jet noise from Strombolian (and Vulcanian) explosions. *Geophysical Research Letters*, *41*(9), 3096-3102.

Vergniolle, S., & Brandeis, G. (1994). Origin of the sound generated by Strombolian explosions. *Geophysical Research Letters*, *21*(18), 1959-1962.

Vergniolle, S., Brandeis, G., & Mareschal, J. C. (1996). Strombolian explosions: 2. Eruption dynamics determined from acoustic measurements. *Journal of Geophysical Research: Solid Earth*, *101*(B9), 20449-20466.

Young, S. M., Gee, K. L., Neilsen, T. B., & Leete, K. M. (2015). Outdoor measurements of spherical acoustic shock decay. *The Journal of the Acoustical Society of America*, *138*(3), EL305-EL310.

5 Appendix A

Materials:

Loctite Liquid Calk

Wood Glue

1 ½" thick 4 ft x 8 ft 'Sound Choice' brand soundproof sheathing board

1 table saw

22 square feet of 1/8" Thick Mass loaded vinyl at 2lb/ft^2

1 aluminum sheet cutter. Otherwise use a table saw with a composite blade, or blade with less than 50

teeth. Otherwise, a razor blade in a handle.

4 hand held vice grips

1 dense weight, such as a large textbook.

Making the box:

1) Cut your sheathing board to make boards with the following dimensions using a table saw:

- 2 boards of 4 ½" x 7 ½"

- 2 boards of 4 ½" x 8 ½"

- 2 boards of 4 ½" x 10 3/4"

- 2 boards of 4 ½" x 11 3/4"

- 1 board of 8 ½" x 8 ½"

- 1 board of 11 3/4" x 11 3/4"

2) Using wood glue, glue the 4 ½" x 7 ½" boards on the inside of the 4 ½" x 8 ½" boards placed in parallel

like so: (This makes a square 8 ½" x 8 ½" box)

*** Not to Scale

4 1/2 "

7 1/2"

8 1/2"

Make sure the edges of the 10" boards
are between those of the 11" boards
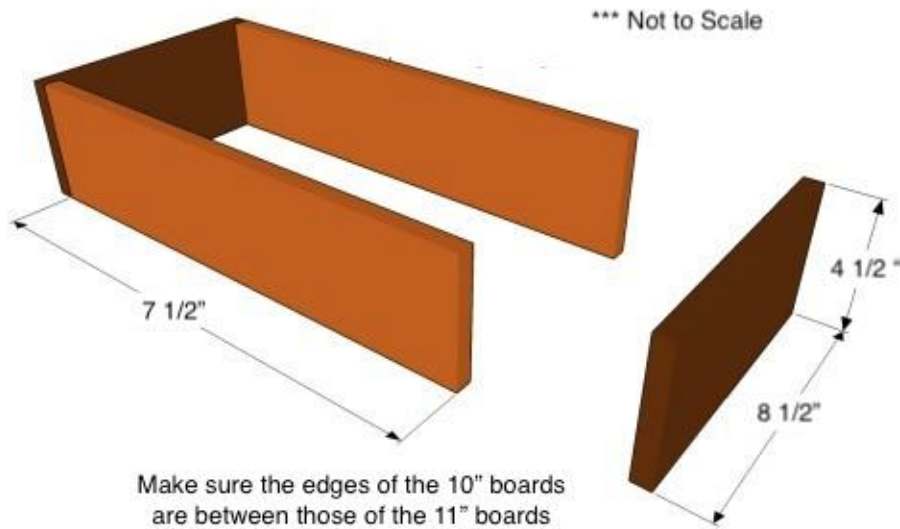
3) Afterwards, glue the 8 ½" x 8 ½" board to the top, making sure the edges are all flush.

4) Use vice grips on the sides to keep the boards in place, and place on a table or the ground with the

top board up. Then place your dense weight on the top of your box and let dry for 30 minutes. (NOTE:

be sure to clean the edges of your box with a paper towel where glue seeps out. If not, your vice grips

may stick to your box. In that event, a sharp knife may be required to cut the glue between the box and

vice grips)

5) (NOTE: if you have enough vice grips, complete this step immediately after step 4. If not, wait 30

minutes for the glue to dry and use the vice grips from the first box)

Glue one of the 13" boards to the two 12" boards with the 12" boards on the inside edge of the 13" (the

same as 10" boards on the inside edges of the 11" boards) and glue the 13" x 13" board on top.

6) Cut the vinyl according to the following chart and keep in piles of the same length:

Quantity	Length (inches)	Height (inches)
2	8.5	4.25
2	8.75	4.25

4	9	4.25
4	9.25	4.25
4	9.5	4.25
4	9.75	4.25
4	10	4.25
4	10.25	4.25
4	10.5	4.25
8	10.75	10.75

7) sort the vinyl into four piles, with 1 sheet of each length, that are in increasing or decreasing order of size. (NOTE: Two piles will have a sheet of 8.75" and the other two with 8.5" long sheets)

8) Once your box with three sides is dried, turn it upside down on the floor or a table, with the 11 3/4" x 11 3/4" side on the ground.

9) place all 10.75" x 10.75" sheets into the open box, then place the smaller box upside down directly on top of the stack of sheets.

10) Fill in the empty space with the stack of vinyl you have by centering them, so they form a pyramid profile, and sliding them in so the larger pieces are adjacent to the sides of the larger box. Leave the empty side for last.

11) When filling in the empty side, add glue to the outside edges of the larger box where the last side fits in. Place the vinyl, then the board to close the box. Use your vice grips to hold it in place for 30 minutes.

(NOTE: the vinyl is loose and can fall out. To prevent this, squeeze some Loctite on the vinyl and spread it out to lightly cover the edges of the vinyl.)

6 Appendix B – Kestral Data of Pretest

Kestrel 1

Time	Crater	ID#	Temp	Humidity	Pressure	Windspeed	Temp
9:43 AM	N	1	30.77	40.60	865.00	1.19	28.21
9:46 AM	N	2	29.36	39.57	864.99	1.09	28.09
10:38 AM	NC	3	30.57	36.74	864.76	1.94	29.70
11:03 AM	NC	4	31.54	33.11	864.90	2.39	30.09
1:18 PM	SC	5	32.34	36.51	863.70	2.63	31.20
1:28 PM	SC	6	32.21	33.14	863.50	2.49	31.33
2:07 PM	S	8	34.17	34.63	862.73	1.77	31.87
2:14 PM	S	9	34.07	31.77	862.70	1.36	32.00
6:31 PM	S	10	28.94	42.33	861.50	1.07	28.21
6:32 PM	SC	11	29.04	41.29	861.50	1.21	28.21
6:43 PM	NC	12	27.84	50.73	861.50	1.09	28.06
6:44 PM	N	13	27.91	49.86	861.50	1.23	28.20
7:50 PM	S	14	26.76	54.06	861.93	1.07	26.86
7:52 PM	SC	15	26.89	54.91	861.93	0.96	26.99
7:55 PM	NC	16	27.09	55.06	861.89	0.76	27.33
7:55 PM	N	17	27.09	55.06	861.89	0.76	27.33
7:59 PM	center (grc	18	27.27	50.37	861.76	1.81	26.97
8:03 PM	center (grc	19	27.00	51.30	861.79	1.66	26.76

7 Appendix C - Code Used

Figure 9- PlotWaveforms.m

Figure 11- Reverb_SPectrum_Plots.m (as spelled)

Figure 12 – Insertion_Loss.m

Figure 13- PlotSpectraBalloons_IL